# Atomic-Scale Insight into LaFeO3 Perovskite: Defect Nanoclusters and Ion Migration

**ARTICLE** *in* THE JOURNAL OF PHYSICAL CHEMISTRY C · MARCH 2008

Impact Factor: 4.77 · DOI: 10.1021/jp710463x

# Atomic-Scale Insight into $LaFeO_3$ Perovskite: Defect Nanoclusters and Ion Migration

**Alison Jones and M. Saiful Islam***

*Department of Chemistry, University of Bath, Bath, BA2 7AY United Kingdom*

*Received: October 30, 2007; In Final Form: January 10, 2008*

Atomistic simulation techniques are employed to investigate the energetics of defect formation, dopant−defect association, and ion migration in orthorhombic $LaFeO_3$ in relation to electrochemical applications. Point defect calculations suggest that intrinsic Schottky or Frenkel disorder is not significant. The results of redox reaction calculations suggest that at high oxygen partial pressures doped $LaFeO_3$ will oxidize with the formation of holes, contributing to the p-type electronic conductivity that is observed experimentally. The binding energies of selected dopant-vacancy clusters are also derived. A minimum in the binding energy was found for $Sr^{2+}$ on the $La^{3+}$ site, which would be beneficial to oxide ion conductivity. Larger complex defect clusters within 2D and 3D configurations have also been considered as they may be important as precursors to possible short-range ordering or "nanodomain" formation. A number of different pathways for oxygen migration by a vacancy mechanism are investigated; the lowest activation energy for this process is via a curved path between oxygen sites. We also examine cation-vacancy transport in $LaFeO_3$ and determine the migration energies for La and Fe migration.

## 1. Introduction

The development of cathode materials for solid oxide fuel cells (SOFCs) has largely focused on perovskite oxide materials with chemical formula $ABO_3$, containing La and Sr on the A sites and transition metals on the B sites. Strontium-doped lanthanum manganate (LSM), $La_{1-x}Sr_xMnO_3$, is the most commonly used cathode material for zirconia-based SOFCs.[1] A key requirement for the development and application of SOFC technologies is to reduce the operating temperature to ≤700 °C[2]. However, at lower temperatures, cell performance may be affected by reduced electrocatalytic reaction at the cathode. In order to improve cathode performance at lower temperatures a number of substituted perovskites, such as lanthanum ferrites, have been considered.[3,4] They have the advantage of higher catalytic activity at lower temperatures, resulting in an overall superior electrochemical performance compared to LSM.[5]

Over a wide range of temperatures and pressures $LaFeO_3$ has been shown to be a mixed oxide ion and electron hole conductor.[6,7] The doped system $La_{1-x}Sr_xFeO_{3-\delta}$ has been extensively studied[8−10] and found to have good p-type electrical conductivity[11] (>100 $Scm^{-1}$); the high electronic and ionic conductivities combined with thermal stability[12] makes them candidate materials as cathodes for SOFCs. However, the defect and ion transport properties of the doped $LaFeO_3$ system are not fully understood.

In this study, orthorhombic $LaFeO_3$, the end member of the solid solution $La_{1-x}Sr_xFeO_{3-\delta}$, which is stable up to approximately 1000 °C,[13] has been probed at the atomic level by employing advanced computer simulation techniques. In this way, the defect chemistry and the mechanism and energetics of ion migration within these perovskite-type materials have been investigated. In addition to this, the substitution of a range of dopants has been investigated together with the energetics of dopant-vacancy clusters.

* Corresponding author. Tel: +44-1225-384938. Fax +44-1225-386231. E-mail: m.s.islam@bath.ac.uk.

## 2. Simulation Methods

The computational techniques used in this work, embodied in the GULP code,[14] are well established and have been reviewed in detail elsewhere.[15,16] The calculations are based upon the Born model of a solid which includes a long-range Coulombic interaction between each pair of ions *i* and *j*, and a short-range Buckingham term to model overlap repulsions and van der Waals forces. The short-range interactions are modeled with a Buckingham potential of the form

$$V_{ij}(r) = A_{ij}\exp(-r/\rho_{ij}) - C_{ij}/r^6 \quad (1)$$

where $A_{ij}$, $\rho_{ij}$, and $C_{ij}$ are the potential parameters and $r$ is the interatomic separation.

The electronic polarizability of the ions is described by the shell model,[17] which has been found to be effective in simulating the dielectric and lattice dynamical properties of metal oxides.[16] Using this model, the deformable ion is represented as a massive core connected by a harmonic spring to a massless, but charge-bearing, shell. The calculation of defect formation and migration energies utilizes the two-region Mott−Littleton methodology[18] for accurate modeling of defective lattices. This is performed such that lattice relaxation occurs about the point defect, or migrating ion, so that the crystal is not considered as a rigid lattice. It employs a method in which the crystal lattice is partitioned into two main regions. Ions in the spherical inner region surrounding the defect are relaxed explicitly, with each ion allowed to relax from its ideal position in order to minimize forces. In the remainder of the crystal, where the defect forces are relatively weak, only implicit polarization of each sublattice is considered, instead of individual ions. A radius of 12 Å was used for the inner region and this typically corresponded to around 550 ions.

## 3. Results and Discussion

**3.1. Structural Modeling.** Unlike the cubic perovskite structure, which only has one distinct oxygen site, the orthor-

10.1021/jp710463x CCC: $40.75 
Published on Web 03/05/2008

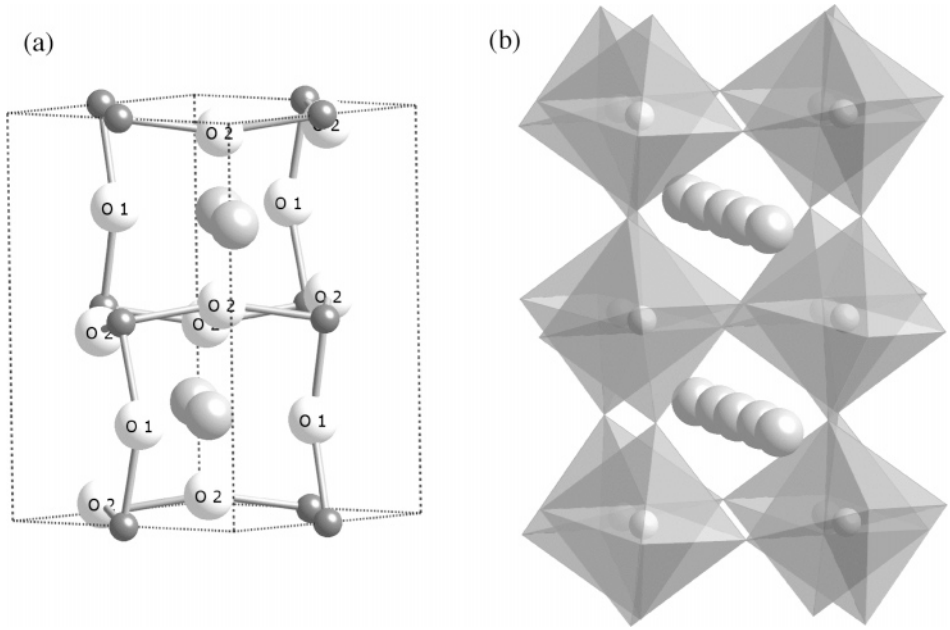


**Figure 1.** (a) Unit cell of orthorhombic $LaFeO_3$ showing the two oxygen sites, O1 and O2; (b) Structure of orthorhomibic $LaFeO_3$ showing the tilted $FeO_6$ octahedra with the La ions occupying the cavities between the octahedra.

**TABLE 1: Interatomic Potential Parameters for $LaFeO_3$ and Dopant Species**

(i) Short-Range Potential

| interaction | *A*/eV | *ρ*/Å$^6$ | *C*/eV Å$^6$ |
|---|---|---|---|
| $La^{3+}\cdots O^{2-}$ | 1545.21 | 0.3590 | 0 |
| $Fe^{3+}\cdots O^{2-}$ | 1156.36 | 0.3299 | 0 |
| $O^{2-}\cdots O^{2-}$ | 22764.30 | 0.1490 | 43.0 |
| $Mg^{2+}\cdots O^{2-}$ | 821.60 | 0.3242 | 0 |
| $Ca^{2+}\cdots O^{2-}$ | 1228.90 | 0.3372 | 0 |
| $Sr^{2+}\cdots O^{2-}$ | 1400.00 | 0.3500 | 0 |
| $Ga^{3+}\cdots O^{2-}$ | 2901.12 | 0.2742 | 0 |
| $Mn^{3+}\cdots O^{2-}$ | 1267.50 | 0.3214 | 0 |
| $Co^{3+}\cdots O^{2-}$ | 1329.82 | 0.3087 | 0 |

(ii) Shell Model[a]

| species | *Y*/e | *k*/eV Å$^{-2}$ |
|---|---|---|
| $La^{3+}$ | −0.25 | 145.0 |
| $O^{2-}$ | −2.24 | 42.0 |
| $Mg^{2+}$ | 2.00 | 99999 |
| $Ca^{2+}$ | 1.26 | 34.00 |
| $Sr^{2+}$ | 1.33 | 21.53 |
| $Ga^{3+}$ | 3.00 | 99999 |
| $Mn^{3+}$ | 3.00 | 95.00 |
| $Co^{3+}$ | 2.04 | 196.30 |

[a] *Y* and *k* refer to the shell charge and harmonic force constant, respectively.

hombic phase of $LaFeO_3$ has two nonequivalent oxygen sites, O1 and O2, as shown in Figure 1a. The structure can be viewed as a network of tilted, corner-sharing $FeO_6$ octahedra with the La cations occupying the cavities between the octahedra as shown in Figure 1b.

The short-range potential parameters and the shell-model parameters for $O^{2-}$ and $La^{3+}$ used in this study (listed in Table 1) were those derived by Cherry et al.[19] in a study of $LaBO_3$ perovskites ($B$ = Cr, Mn, Fe, and Co) by empirical fitting to observed structural properties. The same potential parameters were used for the $Fe^{3+}$ species, but it was assumed to be nonpolarizable and treated simply as a rigid ion. Using this set of interatomic potentials it was possible to reproduce the orthorhombic structure of $LaFeO_3$. The calculated bond distances, lattice parameters, and their comparison with experimental values[20] are listed in Table 2. It can be seen that there is good agreement between experimental and simulated structures, thus supporting the validity of the potentials used for the subsequent defect and migration calculations.

**TABLE 2: Calculated and Experimental Properties of Orthorhombic $LaFeO_3$**

(i) Unit-Cell Parameters

| parameter | calculated/Å | experimental[a]/Å | difference/% |
|---|---|---|---|
| *a* | 5.600 | 5.565 | 0.63 |
| *b* | 7.862 | 7.855 | 0.08 |
| *c* | 5.557 | 5.556 | 0.01 |

(ii) Bond Lengths

| | distance | | |
|---|---|---|---|
| bond separation | calculated/Å | experimental[a]/Å | difference/Å |
| La−O1 | 2.555 | 2.593 | −0.038 |
| La−O2 | 2.438 | 2.651 | −0.213 |
| Fe−O1 | 2.007 | 2.002 | 0.005 |
| Fe−O2 | 2.013 | 2.008 | 0.005 |
| O1−O1 | 3.447 | 3.433 | 0.014 |
| O2−O2 | 3.363 | 3.315 | 0.048 |

[a] Falcon et al.[20]

The interatomic potentials for the dopant species (Table 1) were those of the corresponding binary metal oxides,[21] as they are consistent with the above derived potentials and have successfully been applied to similar studies of dopant substitution in other perovskites.[19,22,23]

**3.2. Intrinsic Atomic Defects.** The energies of isolated intrinsic defects (interstitials and vacancies) in orthorhombic $LaFeO_3$ were first evaluated. It is found that the difference in energy between an O1 and O2 oxygen vacancy is only 0.04 eV. This is not surprising as they occupy similar environments within the orthorhombic $LaFeO_3$ structure as can be seen in Figure 1a.

Frenkel disorder, full Schottky disorder and partial Schottky disorder energies were calculated by combining the individual defect energies and the lattice energies where appropriate. These defect reactions are given below (eqs 2−7) and the corresponding energies listed in Table 3.

**TABLE 3: Calculated Energies for Frenkel- and Schottky-Type Disorder in Orthorhombic $LaFeO_3$**

| disorder | total energy/eV | energy/eV per defect |
|---|---|---|
| La Frenkel | 19.57 | 9.79 |
| Fe Frenkel | 17.13 | 8.57 |
| O Frenkel | 8.49 | 4.25 |
| $LaFeO_3$ full Schottky | 17.49 | 3.60 |
| $La_2O_3$ partial Schottky | 15.15 | 3.03 |
| $Fe_2O_3$ partial Schottky | 18.50 | 3.70 |

Lanthanum Frenkel disorder:

$$La_{La}^{X} \leftrightarrow V_{La}^{///} + La_{i}^{\bullet\bullet\bullet} \quad (2)$$

Iron Frenkel disorder:

$$Fe_{Fe}^{X} \leftrightarrow V_{Fe}^{///} + Fe_{i}^{\bullet\bullet\bullet} \quad (3)$$

Oxygen Frenkel disorder:

$$O_{O}^{X} \leftrightarrow V_{O}^{\bullet\bullet} + O_{i}^{//} \quad (4)$$

$LaFeO_3$ full Schottky disorder:

$$La_{La}^{X} + Fe_{Fe}^{X} + 3O_{O}^{X} \leftrightarrow V_{La}^{///} + V_{Fe}^{///} + 3V_{O}^{\bullet\bullet} + LaFeO_3 \quad (5)$$

$La_2O_3$ partial Schottky disorder:

$$2La_{La}^{X} + 3O_{O}^{X} \leftrightarrow 2V_{La}^{///} + 3V_{O}^{\bullet\bullet} + La_2O_3 \quad (6)$$

$Fe_2O_3$ partial Schottky disorder:

$$2Fe_{Fe}^{X} + 3O_{O}^{X} \leftrightarrow 2V_{Fe}^{///} + 3V_{O}^{\bullet\bullet} + Fe_2O_3 \quad (7)$$

where, in Kröger−Vink notation,[24] $O_i^{//}$, $La_i^{\bullet\bullet\bullet}$, and $Fe_i^{\bullet\bullet\bullet}$ represent oxygen, lanthanum, and iron interstitials, respectively, $V_O^{\bullet\bullet}$, $V_{La}^{///}$, and $V_{Fe}^{///}$ represent oxygen, lanthanum, and iron vacancies, respectively, and the superscripts $^{\bullet}$ (positive), $^{/}$ (negative), and $^{x}$ (neutral) indicate the charge of the defect relative to the normal site.

The Frenkel disorder energies are much higher than the other disorder energies. The results suggest that interstitials would be unlikely intrinsic defects (as would be expected in a close-packed perovskite structure). The lowest energy is for the $La_2O_3$ Schottky-type disorder. However, the Schottky energies are still relatively high, suggesting that we would not expect intrinsic Schottky or Frenkel disorder to dominate the defect chemistry of undoped stoichiometric $LaFeO_3$ except at very high temperatures. This is consistent with the defect models proposed by Mizusaki et al.[11] in a study of $La_{1-x}Sr_xFeO_{3-\delta}$ ($x = 0.0$, 0.1, and 0.5). It is interesting to note that Wærnhus et al.[7,25] have investigated the non-stoichiometric system $La_{1-y}FeO_{3-\delta}$; they proposed that the *p*-type conductivity at high oxygen partial pressures is due to the formation of Schottky defects at high annealing temperatures (>1000 °C) and that the number of cation vacancies, which act as electron acceptors and introduce p-type conductivity, will increase with the oxygen partial pressure; this issue warrants further investigation.

**3.3. Redox Reactions.** An understanding of the redox behavior of these materials is critical for defining the conditions in which various conductivity regimes may be exploited. Mizusaki et al.[11] have described the electronic conductivity as localized electrons and holes hopping between the Fe ions of different valence states. Studies on the electronic properties of $LaFeO_3$ suggest that the *n*-type conductivity at low oxygen partial pressures is due to reduction of $Fe^{3+}$ to $Fe^{2+}$ and the formation of oxygen vacancies.

Experimental determination and interpretation of the defect equilibria are complicated due to the number of possible conducting species (oxide ion, electron or hole). Atomistic simulation is therefore a useful tool in assisting the interpretation of experimental data, as has been shown previously.[22]

Using an approach that has been successfully applied to other transition metal oxides,[26] the electronic defects, electrons ($e'$) and holes ($h^{\bullet}$), were treated as localized species (small polarons). The hole species was assumed to reside on either an oxide ion ($O^{2-} \rightarrow O^{-}$) or iron ion ($Fe^{3+} \rightarrow Fe^{4+}$). Oxidation and reduction in undoped $LaFeO_3$ were considered (eqs 8−11), and the energies of these processes compared with that of the doped system in order to determine the most likely oxidation and reduction mechanisms. For the undoped system, the following reactions were considered:

(i) Oxidation to give a metal deficient material:

$$\frac{1}{2}O_2\,(g) + \frac{2}{3}Fe_{Fe}^{x} \rightarrow \frac{2}{3}V_{Fe}^{///} + 2h^{\bullet} + \frac{1}{3}Fe_2O_3 \quad (8)$$

or

$$\frac{1}{2}O_2\,(g) + \frac{2}{3}La_{La}^{x} \rightarrow \frac{2}{3}V_{La}^{///} + 2h^{\bullet} + \frac{1}{3}La_2O_3 \quad (9)$$

With regard to the hole species, our calculations found that the formation of an $O^{-}$ species is more favorable than $Fe^{4+}$ formation by about 3 eV, suggesting that holes are more likely to be centered on oxygen sites, although we recognize that there will be some degree of Fe(3d)−O(2p) mixing.[27]

(ii) Reduction to give an oxygen deficient material was the only one considered, as introduction of cation interstitials has been shown to be an energetically unfavorable process:

$$O_{O}^{x} \rightarrow V_{O}^{\bullet\bullet} + \frac{1}{2}O_2\,(g) + 2e^{/} \quad (10)$$

(iii) We also examined the energetics of disproportionation of two $Fe^{3+}$ ions to $Fe^{2+}$ and $Fe^{4+}$ ions according to the equation:

$$2Fe_{Fe}^{x} \rightarrow Fe_{Fe}^{\bullet} + Fe_{Fe}^{/} \quad (11)$$

$M^{2+}$ dopants may be substituted into the $LaFeO_3$ structure in order to introduce vacancies at oxygen sites. At high oxygen partial pressures, doping can also be used to affect electronic conductivity by "filling" of the oxygen vacancies to create holes ($h^{\bullet}$). The energetics of hole formation in doped $LaFeO_3$ were examined via the following reaction:

$$\frac{1}{2}O_2 + V_{O}^{\bullet\bullet} \rightarrow O_{o}^{x} + 2h^{\bullet} \quad (12)$$

The energies of the various redox processes, summarized in Table 4, were calculated using the appropriate free ion terms together with the point defect energies and the relevant lattice energies.

The results indicate that the most favorable redox process is oxidation of doped $LaFeO_3$ with the formation of holes (eq 12). The calculations therefore suggest that p-type conduction would be exhibited in the doped $LaFeO_3$ system at high oxygen partial pressures, as found experimentally.[4,11] This process is important for mixed ionic-electronic conductivity in doped $LaFeO_3$ and its potential use in SOFC cathodes or ceramic membranes. In the undoped stoichiometric system, however, both oxidation and

**TABLE 4: Calculated Energies of Redox Reactions**

| process | eq | energy/eV per electronic defect[a] |
|---|---|---|
| oxidation | 8 | 5.94 |
| oxidation | 9 | 5.38 |
| reduction | 10 | 4.69 |
| disproportionation | 11 | 5.23 |
| oxidation | 12 | 2.86 |

[a] Calculated using $\Delta E = 9.87$ eV for $1/2O_2 \rightarrow O^{2-}$; O hole ($h^{\bullet}$) term = 7.65 eV; Fe hole ($h^{\bullet}$) term = 10.56 eV; Fe electron (e') term = −0.11 eV.

reduction energies indicate relatively unfavorable processes. The calculated energy for disproportionation suggests that this too is an unlikely process in $LaFeO_3$, in contrast to some Co-based perovskites.[28]

**3.4. Dopant-Vacancy Association.** The oxygen vacancies which are formed as a result of acceptor-doping of $ABO_3$ perovskites have been shown to be crucial to high oxygen conductivity in perovskite materials.[29] Misuzaki et al.[30] have pointed out that the diffusivity of oxygen in La perovskites is controlled by the oxygen vacancy concentration. Interactions between dopant ions and their charge compensating defects can lead to the formation of distinct clusters which can trap the migrating species. A recent review of fast oxygen transport in acceptor-doped oxides[31] concluded that there is a dopant concentration dependence in the conductivity and the activation enthalpy of doped oxides. It has also been noted that there is a minimum in the activation enthalpy which may be an indicator of dopant-vacancy association.

In fluorite-structured oxides (e.g., doped $CeO_2$ and $ZrO_2$), interactions between dopant ions and their oppositely charged compensating defects lead to the formation of defect clusters or associates.[31,32] This adds a binding (association) energy term to the conduction activation energy. Dielectric relaxation measurements of acceptor-doped $KTaO_3$ and $CaTiO_3$ perovskites by Nowick et al.[33] also provide evidence of dopant-vacancy pairs.

A series of calculations on defect clusters in orthorhombic $LaFeO_3$ were carried out to investigate interactions between oxygen vacancies and dopant cations, which are not fully understood in this material. For this task, the simulation methods used here are well suited as they model accurately Coulomb and polarization energies, which are the predominant terms in any local association process.

Work on the $LaGaO_3$ perovskite[34] suggests that in addition to the electrostatic attraction, the elastic energy term due to distortion of the crystal lattice upon introduction of different-sized cations contributes to cluster formation, as found in fluorite oxides.

In this study, a number of different dopant-vacancy configurations (pairs and trimers) were simulated to ascertain whether any degree of "trapping" of the oxygen vacancies by the dopant species might occur. At higher dopant concentrations, there is the possibility that an oxygen vacancy may be associated with one or more dopant cations; therefore, the association of both charged dimers ($M'V_o^{\bullet\bullet}$) and neutral trimers ($M'V_o^{\bullet\bullet}M'$) has been studied. The configurations that were considered for the pair clusters are comprised of an $M^{2+}$ or $M^{3+}$ dopant substitutional and either an O1 or O2 oxygen vacancy at nearest neighbor sites. For the neutral trimer clusters, two $M^{2+}$ dopant substitutionals and the nearest neighbor O1 or O2 vacancy were considered.

**TABLE 5: Calculated Binding Energies for $M^{2+}$ Dopant-Oxygen Pair-Clusters and $M^{2+}$ Neutral Trimer Clusters ($M'V_o^{\bullet\bullet}M'$) at (a) the La Site and (b) the Fe Site, and (c) $M^{3+}$ Dopant-Oxygen Pair-Clusters at the Fe Site in $LaFeO_3$**

(a) $M^{2+}$ on La Site

| dopant | mean binding energy/eV per defect | |
|---|---|---|
| $M^{2+}$ and O1 vacancy | $(M'_{La}V_o^{\bullet\bullet})$ pair | $(M'_{La}V_o^{\bullet\bullet}M'_{La})$ trimer |
| $Ca^{2+}$ | −0.22 | −0.35 |
| $Sr^{2+}$ | −0.17 | −0.33 |
| $M^{2+}$ and O2 vacancy | | |
| $Ca^{2+}$ | −0.33 | −0.34 |
| $Sr^{2+}$ | −0.31 | −0.32 |

(b) $M^{2+}$ on Fe Site

| dopant | mean binding energy/eV per defect | |
|---|---|---|
| $M^{2+}$ and O1/O2 vacancy | $(M'_{Fe}V_o^{\bullet\bullet})$ pair | $(M'_{Fe}V_o^{\bullet\bullet}M'_{Fe})$ trimer |
| $Mg^{2+}$ | −0.54 | −0.69 |

(c) $M^{3+}$ on Fe site

| dopant | mean binding energy/eV per defect |
|---|---|
| $M^{3+}$ and O1/O2 vacancy | $(M^x_{Fe}V_O^{\bullet\bullet})$ pair |
| $Ga^{3+}$ | 0.17 |
| $Mn^{3+}$ | 0.00 |
| $Co^{3+}$ | −0.10 |

The cluster binding energies ($E_{bind}$) were calculated using the general relation:

$$E_{bind} = E_{cluster} - \left( \sum_{component} E_{isolated\ defect} \right) \qquad (13)$$

where $E_{cluster}$ is the energy of the cluster and $E_{isolated}$ is the energy of the individual component defects. For example, the binding energy for the $(Mg'_{Fe}V_o^{\bullet\bullet})$ pair cluster is derived as follows:

$$E_{bind} = E(Mg'_{Fe}V_o^{\bullet\bullet}) - [E(Mg'_{Fe}) + E(V_o^{\bullet\bullet})] \qquad (14)$$

A negative value indicates that the cluster is stable with respect to the isolated defects.

In this study we focused on dopants typically used in these systems, namely $Ca^{2+}$ and $Sr^{2+}$ on the $La^{3+}$ site, and $Mg^{2+}$, $Ga^{3+}$, $Mn^{3+}$, and $Co^{3+}$ on the $Fe^{3+}$ site. The results of the calculations for these selected dopants are summarized in Table 5.

It can be seen from Table 5 that the calculated binding energies for $M^{2+}$ dopant pair and trimer clusters all indicate a degree of association at the La or the Fe sites, ranging from −0.17 to −0.69 eV. The smallest binding energies for $M^{2+}$ dopant pair clusters are calculated for $Sr^{2+}$ and $Ca^{2+}$ at the La site and an O1 vacancy. Incorporation of Sr into $LaFeO_3$ would be expected to increase the conductivity owing to the increase in vacancy concentration, and a low binding energy would be a major factor in promoting the free oxygen vacancy population. High oxygen diffusivity with increasing levels of $Sr^{2+}$ substitution is reported by Ishigaki,[10] and other workers have found that the oxygen diffusivity in $La_{1-x}Sr_xFeO_{3-\delta}$ reaches a maximum at $x = 0.3$[9] or 0.5.[35]

The results of these calculations also suggest that Mg has a stronger tendency to "trap" migrating oxygen vacancies than the Sr dopant and that at high Mg doping levels the conduction activation energy is likely to increase. This has been shown to be the case by Haavik et al. for $LaGaO_3$.[36] Their defect model has been used to rationalize the temperature-dependent con-

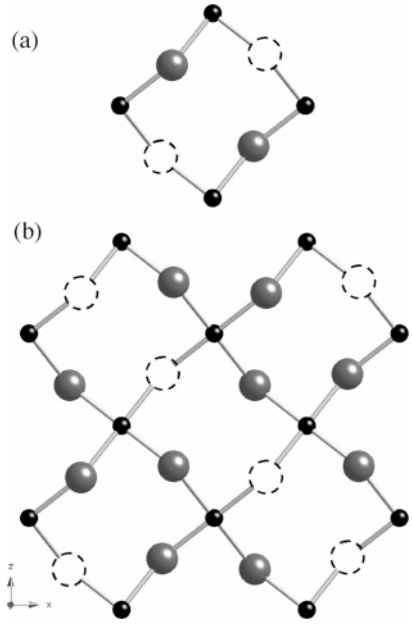


**Figure 2.** Views down [010] of 2D arrays of neutral $Mg^{2+}$-vacancy clusters: (a) $4Mg'_{Fe}2V_o^{\bullet\bullet}$ (b) $12Mg'_{Fe}6V_o^{\bullet\bullet}$ (black spheres and open dashed circles represent Mg dopant ions and oxygen vacancies, respectively).

ductivity of $LaGaO_3$ and derive a defect association enthalpy (≈0.8 eV) of the same order as our calculated binding energy for $LaFeO_3$.

The calculated binding energies for selected $M^{3+}$ dopant pair clusters ($M^x_{Fe}V_O^{\bullet\bullet}$) on the Fe site are also presented in Table 5. These isovalent substitutionals have no effective charge (i.e., relative to the host $Fe^{3+}$ lattice ions). With respect to acceptor dopants, the population of oxygen vacancies would be dependent upon the $M^{2+}$ dopants, e.g., $Sr^{2+}$, already introduced into the lattice. The results indicate a very small degree of association for $Co^{3+}$. Since the binding energy is dependent on the ion size mis-match between host and dopant,[31] these results are not unexpected as the ionic radii of $Mn^{3+}$, $Ga^{3+}$, and $Co^{3+}$ are very close to that of $Fe^{3+}$. It is worth noting that the ionic radius of $Mn^{3+}$ is almost identical to that of $Fe^{3+}$, and the calculated binding energy for the ($Mn^x_{Fe}V_O^{\bullet\bullet}$) cluster is zero. We should note that similar small binding energies are found for $Gd^{3+}$ and $Nd^{3+}$ on the La site, again indicating the importance of elastic strain effects.

**3.5. Complex $Mg^{2+}$-Vacancy Clusters.** Our results for $Mg^{2+}$ dopant pair and trimer clusters suggest the importance of defect-dopant association in relation to conductivity studies. Although simple pair clusters may dominate in the low concentration regime, it is thought that at higher dopant levels more complex defect clusters come into play and may be related to possible short-range ordering.[37]

We have examined the energetics of larger clusters, focusing on Mg on the Fe site with oxygen vacancies at nearest neighbor sites. Neutral configurations based on ($nMg'_{Fe}$ $n/2V_o^{\bullet\bullet}$) were considered, both for two-dimensional (2D) and three-dimensional (3D) clusters with the number of $Mg^{2+}$ dopant ions ($n$) ranging from 2 to 16. Examples of selected 2D and 3D clusters are shown in Figures 2 and 3, respectively. The binding energies are derived by the same methodology described in eqs 13 and 14. The calculated binding energies for all of the configurations examined are presented in Figure 4 as a function of the number of $Mg^{2+}$ ions in the cluster.

All of the clusters show relatively favorable binding energies with the magnitude varying for the different configurations. The strongest binding energy is found for the ($12Mg'_{Fe}6V_o^{\bullet\bullet}$) 3D configuration and in general the 3D structures show greater stability than the 2D arrays. The results suggest that complex nanoscale clusters such as ($12Mg'_{Fe}6V_o^{\bullet\bullet}$) or ($16Mg'_{Fe}8V_o^{\bullet\bullet}$) may form at high dopant concentrations and possibly be important as precursors to possible short-range ordering or "nanodomain" formation. In this context, in a study of $LaGaO_3$, Huang et al.[38] have suggested that dopant ions such as $Mg^{2+}$ may act not only as traps for isolated oxygen vacancies, but also as nucleating centers for the formation of ordered vacancy clusters. Such defect clusters in doped $LaFeO_3$ warrant further structural study.

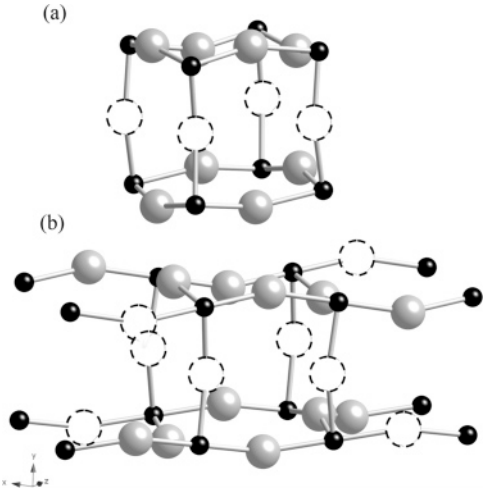


**Figure 3.** 3D configurations of neutral $Mg^{2+}$-vacancy clusters: (a) $8Mg'_{Fe}4V_o^{\bullet\bullet}$ (b) $16Mg'_{Fe}8V_o^{\bullet\bullet}$ (black spheres and open dashed circles represent Mg dopant ions and oxygen vacancies, respectively).

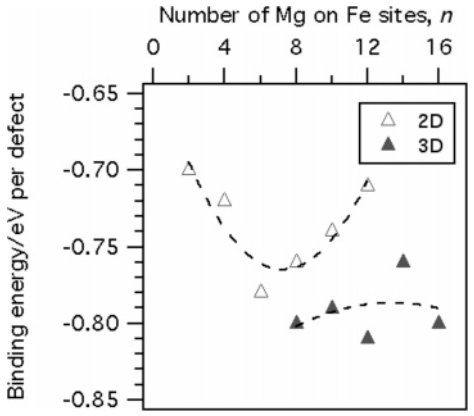


**Figure 4.** Calculated binding energies for 2D and 3D configurations of neutral $Mg^{2+}$-vacancy clusters ($nMg'_{Fe}n/2V_o^{\bullet\bullet}$) as a function of the number of $Mg^{2+}$ ions, $n$. Lines are a guide to the eye only.

**3.6. Oxide-Ion Migration.** The presence of the two non-equivalent O1 and O2 oxygen sites in orthorhombic $LaFeO_3$ means that three possible vacancy migration pathways can be identified. The energy profiles for oxide ion migration were mapped out by calculating the defect energy of the migrating ion at intermediate sites between adjacent oxygen vacancies, allowing relaxation of the lattice ions at each position. In the saddlepoint configuration, the migrating oxide ion must pass through the opening of a triangle defined by two $La^{3+}$ ions and one $Fe^{3+}$ ion (Figure 5). Significant outward relaxation of these cations away from the migrating oxide ion is found. The simulations indicate the importance of local lattice relaxation effects and that the saddlepoint cannot be treated purely as a structural gap of hard-sphere ions.

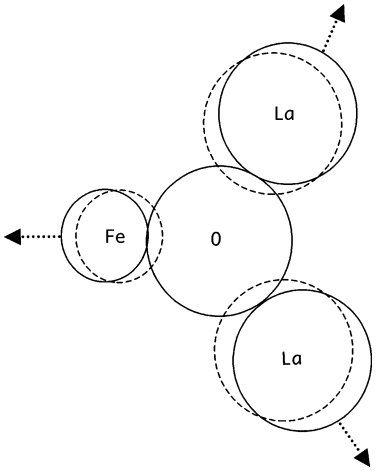


**Figure 5.** Saddlepoint configuration for oxide ion migration indicating the relaxation of the surrounding cations (solid lines). Dashed circles represent the unrelaxed positions of the cations.

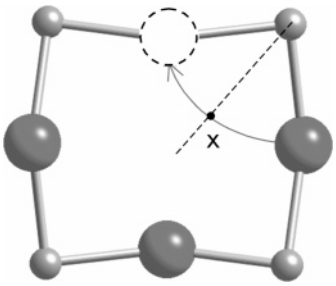


**Figure 6.** Schematic representation of the calculated pathway (curved line) of oxide ion migration between occupied and vacant O2 sites. The position of the saddlepoint is shown with a cross. Small gray spheres represent Fe ions.

**TABLE 6: Calculated Migration Energy ($E_m$) for Oxide Ion Migration in $LaFeO_3$ and Total Calculated Activation ($E_a$) in Sr-Doped $LaFeO_3$**

| migration pathway | separation/ Å | calculated $E_m$/eV | Sr binding energy term/ eV | total calculated $E_a$/eV |
|---|---|---|---|---|
| O1−O1 | 3.43 | 2.13 | 0.17 | 2.30 |
| O1−O2 | 2.80 | 0.44 | 0.26 | 0.70 |
| O2−O2 | 2.80 | 0.50 | 0.34 | 0.84 |

For oxygen migration between two O2 sites or between an O1 and O2 site, it was found that the lowest energy pathway was a curved path, as shown in Figure 6, away from the octahedral edge, as has been found previously for oxygen migration in cubic $LaGaO_3$ and other perovskite oxides.[15,22,39] Subsequent neutron scattering and diffraction studies[40] have provided evidence for our predicted curved path. However, for oxygen migration between two O1 vacancies, the lowest energy migration pathway was found to be a direct linear route between the two sites. The results (Table 6) clearly show that migration between O1 sites is extremely unlikely, but a pathway linking O2 sites or between O2 and O1 sites with a migration energy, $\Delta E_m$, of 0.5 eV is energetically very favorable.

It is important to stress that the calculated migration energies relate purely to migration of an oxygen vacancy and do not include a binding term. The values calculated here do not take into account the dopant-vacancy association which may contribute to the observed activation energies. Inclusion of the binding energy term in the calculated energy for oxygen migration in Sr-doped $LaFeO_3$ results in a calculated activation energy of between 0.70 and 0.84 eV (Table 6).

**TABLE 7: Reported Experimental Activation Energies for Oxide Ion Conduction in $La_{1-x}Sr_xFeO_{3-\delta}$**

| $x$ | $E_a$/eV | temp. range/°C | ref |
|---|---|---|---|
| 0.0 | 0.77 | 900−1100 | 41 |
| 0.1 | 0.88 | 900−1100 | 10 |
| 0.1 | 1.17 | 850−1050 | 9 |
| 0.2 | 1.67 | 850−1050 | 9 |
| 0.3 | 1.80 | 850−1050 | 9 |
| 0.4 | 1.56 | 850−1050 | 9 |
| 0.2 | 0.67 | 750−950 | 35 |
| 0.4 | 0.67 | 750−950 | 35 |
| 0.5 | 0.70 | 750−950 | 35 |

Activation energies for oxide ion transport via vacancy migration determined experimentally at low oxygen partial pressures and 950 °C range from 0.67 eV in $La_{1-x}Sr_xFeO_{3-\delta}$ for $0.2 \leq x \leq 0.5$[35] to 0.77 eV for $LaFeO_3$.[41] These results are consistent with a model proposed by Haavik et al.[36] for $LaGaO_3$ in which they rationalize the temperature dependence of conductivity in terms of dopant-oxygen vacancy clusters.

Patrakeev et al.[35] have reported that at low oxygen partial pressures the oxide ion conductivity increases to a maximum value at $x = 0.5$ but that the activation energy for ion conductivity does not depend on the Sr content until $x > 0.5$, after which it increases with increasing Sr content. This increase in activation energy was explained in terms of vacancy ordering, which decreases the population of oxygen vacancies available for oxygen transport.

We recognize that direct comparison between the migration energies calculated here and the experimental activation energies ($E_a$) is not straightforward since the $E_a$ values (listed in Table 7) from a range of conductivity studies on both $LaFeO_3$ and $La_{1-x}Sr_xFeO_{3-\delta}$ show significant variation. This may reflect differences in the synthesis conditions and phase purity or the method of determination and analysis of conductivity data.

Finally, we investigated the possibility of association between oppositely charged lanthanum and oxygen vacancies which could occur in A-site deficient compositions. Our calculated binding energy for the $(V_{La}^{///}V_O^{\bullet\bullet})$ pair cluster is found to be −1.02 eV per defect. This strong binding energy suggests that this could be a factor inhibiting the mobility of oxygen vacancies. As it has been proposed that the dominant compensation mechanism for A-site deficiency in lanthanum ferrites and cuprates is *via* the formation of oxygen vacancies,[4,42,43] such a defect association would be expected to have a detrimental effect on the conductivity of these materials. However, it has been shown that La deficiency in the related $LaMnO_3$ system has no effect on oxygen diffusion compared to the cation stoichiometric compound.[44] This was attributed to the fact that the formation of negatively charged La vacancies, $V_{La}^{///}$, is compensated by the oxidation of $Mn^{3+}$ ions rather than the formation of oxygen vacancies, $V_O^{\bullet\bullet}$. It has also been shown that A-site deficiency plays an important role in enhancing the performance of LSCF cathode materials;[43] therefore, the formation of holes may be the compensating mechanism for La-deficiency in $LaFeO_3$.

**3.7. Cation Migration.** The diffusion of cations is known to be slow compared to that of oxide ions. Cation diffusion may cause chemical creep, demixing, or decomposition and plays a key role in sintering, grain growth, and interactions at the electrode−electrolyte interface.[45,46] The rate at which some of these processes occur is determined by the slowest moving species.[46] If the cations exhibit different diffusivities, kinetic demixing of cations[47] may contribute to the long-term degradation of oxide ion conductors in SOFCs. The energetics of cation migration were therefore investigated by atomic-scale simula-

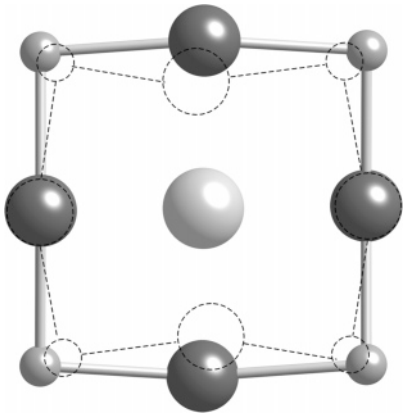

**Figure 7.** View down [010] showing a migrating La ion at the saddle point and the consequent local relaxation of the surrounding ions. The dashed line represents the migration aperture before relaxation.

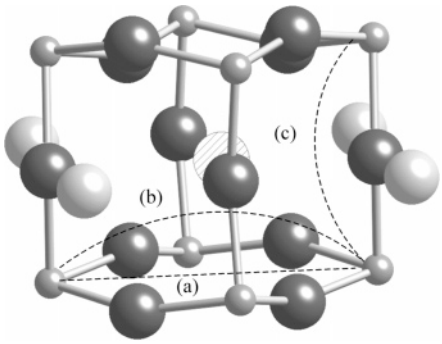


**Figure 8.** Possible pathways for Fe vacancy migration in $LaFeO_3$: (a) linear pathway along [100], (b) curved pathway along [100] with nearest La site vacant (shown as striped sphere) and (c) curved pathway between two Fe sites separated by an oxygen in the [010] direction with the same vacant La site. Small gray spheres represent Fe, large dark spheres O and large gray spheres La.

**TABLE 8: Calculated Activation Energies for Migration of La and Fe Ions in Orthorhombic $LaFeO_3$**

| cation | migration pathway | migration energy/eV |
|---|---|---|
| $La^{3+}$ | linear along [010] | 4.00 |
| $La^{3+}$ | linear along [101] | 4.21 |
| $Fe^{3+}$ | linear along [100] (a)[a] | 13.18 |
| $Fe^{3+}$ | curved pathway with adjacent La vacancy (b)[a] | 6.16 |
| $Fe^{3+}$ | curved pathway in [010] direction with adjacent La vacancy (c)[a] | 3.25 |

[a] See Figure 8

tions of vacancy migration between cation sites for both $La^{3+}$ and $Fe^{3+}$ ions.

Examination of the orthorhombic $LaFeO_3$ structure suggests that the most likely migration route for lanthanum diffusion is a linear pathway between La sites along either [010] or [101] passing through an aperture defined by four oxygen and four Fe ions as shown in Figure 7. As the radius of the $La^{3+}$ ion is larger than the radius of this aperture, the surrounding lattice relaxes substantially in order to allow the migrating $La^{3+}$ ion to pass through when it is at the saddle point. The degree of relaxation is shown in Figure 7 and the channel widens by 0.85 Å as the oxide ions move away from the migrating cation.

The calculated activation energies for La vacancy migration are listed in Table 8. As expected, the migration energy along [101] is greater as the bottleneck width is slightly smaller (3.32 Å versus 3.51 Å for [010]).

Simulation studies of cation migration in $LaGaO_3$[48] and $LaMnO_3$[49] have examined possible migration pathways for the B-site cation in cubic perovskite structures. These are a linear jump in the <110> direction or a more complex <100> jump along a curved pathway between B-cation sites along the $<100>_{cubic}$ direction.

Three pathways were examined for migration of $Fe^{3+}$ in orthorhombic $LaFeO_3$. The results of these calculations are listed in Table 8 and the approximate migration pathways are shown in Figure 8. The first of these (a) was the linear jump between two Fe sites along [100] (the equivalent jump pathway to <110> in the cubic structure). A high migration energy of 13.18 eV was obtained; this is similar to that obtained for the B-site cation migration calculated for $LaGaO_3$ and $LaMnO_3$. The second pathway examined, (b), was also along the [100] direction, but mediated by the presence of a La vacancy on the nearest or next-nearest La site above the migration plane. The Fe ion moved in a curved pathway out of the (010) plane so that it was further from the surrounding oxide ions. Third, in (c), the migrating ion moved up and around the oxide ion located between two Fe sites adjacent along the [010] direction. This is similar to the calculated pathway described for $Mn^{3+}$ migration in $LaMnO_3$.[49] As the migrating ion must pass between an oxide ion and a lanthanum ion at the saddlepoint, a La vacancy was created on the adjacent site. Our calculations find a relatively low energy of 3.25 eV for the third mechanism (c). De Souza and Maier[48] also found that the migration energy for $Ga^{3+}$ in $LaGaO_3$ dropped to 3.84 eV for this type of $V'''_{La}$-mediated migration.

From recent studies of cation self-diffusion in close-to-stoichiometric $LaFeO_3$, Smith and Norby[50] have suggested that the predominant diffusing species is $Fe^{3+}$ with an activation energy of 3.3 eV, and that this represents the sum of the diffusion activation enthalpy and the formation enthalpy of the defect. Our results suggest that this observed activation energy may be purely a diffusion or migration enthalpy, although we recognize that further detailed experimental work on conductivity and computational studies using molecular dynamics (MD) are required. An MD study of doped $LaGaO_3$[51] has suggested that cation diffusion is governed by diffusion via lattice vacancies in a mechanism similar to (b) and (c) above. It was suggested that the diffusion of cations is correlated to the formation and migration of a binary vacancy complex of two neighboring vacancies on the A and B sites of the perovskite lattice.

## 4. Conclusions

Atomistic simulation techniques have been used to probe the energetics of defects, dopants, nanoclustering and ion migration in the lanthanum ferrite $LaFeO_3$. The results have provided information at the atomic level which is relevant to the electrochemical behavior of $LaFeO_3$ and the doped system $La_{1-x}Sr_xFeO_{3-\delta}$ for potential SOFC applications. The main points are summarized as follows:

1. The calculated defect energies suggest that intrinsic disorder of the Frenkel or Schottky type is unlikely except at extremely high temperatures. The lowest energy redox process is oxidation of acceptor-doped $LaFeO_3$ with the formation of electronic holes. This result suggests p-type conduction in doped $LaFeO_3$ will occur at high oxygen partial pressures, as observed experimentally.

2. The binding energies for dopant-oxygen vacancy clusters indicate that Sr doping should enhance oxide-ion conductivity because of the low binding energy and the increase in vacancy

concentration. However, as the $Mg^{2+}$ substitutional has a strong tendency to "trap" the migrating oxygen vacancy, this would be detrimental to oxide-ion conductivity. Large complex clusters ($n\mathrm{Mg}_{\mathrm{Fe}}^{/}$ $n/2\mathrm{V}_{\mathrm{o}}^{\bullet\bullet}$) with $n$ up to 12 or 16 in 2D and 3D configurations, respectively, have been considered. These clusters may be important as precursors to possible short-range ordering or "nanodomain" formation at higher dopant concentrations, and warrants further structural study.

3. The pathway for oxide-ion migration is predicted to be a curved trajectory for O2−O2 or O2−O1 pathways. Inclusion of the binding energy term in the calculated energy for oxygen migration in Sr-doped $LaFeO_3$ results in calculated activation energies of between 0.70 and 0.84 eV. As expected, cation diffusion has high migration energies for both $La^{3+}$ and $Fe^{3+}$ vacancies. The lowest calculated energy (3.25 eV) is for Fe migration involving a La vacancy-mediated mechanism.

**Acknowledgment.** We would like to thank the Daphne Jackson Trust for providing a Research Fellowship funded by the EPSRC.

## References and Notes

(1) Haile, S. M. *Acta Mater.* **2003**, *51*, 5981. Ormerod, R. M. *Chem. Soc. Rev.* **2003**, *32*, 17. Steele, B. C. H.; Heinzel, A. *Nature* **2001**, *414*, 345.

(2) Steele, B. C. H. *Solid State Ionics* **2000**, *134*, 3.

(3) Park, C. Y.; Azzarello, F. V.; Jacobson, A. J. *J. Mater. Chem.* **2006**, *16*, 3624. Simner, S. P.; Bonnett, J. R.; Canfield, N. L.; Meinhardt, K. D.; Shelton, J. P.; Sprenkle, V. L.; Stevenson, J. W. *J. Power Sources* **2003**, *113*, 1. Zhou, X. D.; Yang, J. B.; Thomsen, E. C.; Cai, Q.; Scarfino, B. J.; Nie, Z.; Coffey, G. W.; James, W. J.; Yelon, W. B.; Anderson, H. U.; Pederson, L. R. *J. Electrochem. Soc.* **2006**, *153*, J133. Cheng, J. H.; Navrotsky, A.; Zhou, X. D.; Anderson, H. U. *Chem. Mater.* **2005**, *17*, 2197. Bouwmeester, H. J. M.; Den Otter, M. W.; Boukamp, B. A. *J. Solid State Electrochem.* **2004**, *8*, 599. Naumovich, E. N.; Patrakeev, M. V.; Kharton, V.; Islam, M. S.; Yaremchenko, A. A.; Frade, J. R.; Marques, F. M. B. *Solid State Ionics* **2006**, *177*, 457.

(4) Kharton, V. V.; Waerenborgh, J. C.; Viskup, A. P.; Yakovlev, S. O.; Patrakeev, M. V.; Gaczynski, P.; Marozau, I. P.; Yarermchenko, A. A.; Shaula, A. L.; Samakhval, V. V. *J. Solid State Chem.* **2006**, *179*, 1273.

(5) Mai, A.; Haanappel, V. A. C.; Uhlenbruck, S.; Tietz, F.; Stöver, D. *Solid State Ionics* **2005**, *176*, 1341.

(6) Mizusaki, J.; Sasamoto, T.; Cannon, W. R.; Bowen, H. K. *J. Am. Ceram. Soc.* **1982**, *65*, 363.

(7) Wærnhus, I.; Vullum, P. E.; Holmestad, R.; Grande, T.; Wiik, K. *Solid State Ionics* **2005**, *176*, 2783.

(8) Dann, S. E.; Currie, D. B.; Weller, M. T.; Thomas, M. F.; Al-Rawwas, A. D. *J. Solid State Chem.* **1994**, *109*, 134. Wærnhus, I.; Sakai, N.; Yokokawa, H.; Grande, T.; Einarsrud, M.-A.; Wiik, K. *Solid State Ionics* **2004**, *175*, 69.

(9) ten Elshof, J. E.; Bouwmeester, H. J. M.; Verweij, H. *Solid State Ionics* **1995**, *81*, 97.

(10) Ishigaki, T.; Yamauchi, S.; Kishio, K.; Mizusaki, J.; Fueki, K. *J. Solid State Chem.* **1988**, *73*, 179.

(11) Mizusaki, J.; Sasamoto, T.; Cannon, W. R.; Bowen, H. K. *J. Am. Ceram. Soc.* **1983**, *66*, 247.

(12) Kawada, T.; Yokokawa, H. *Key Eng. Mater.* **1997**, *125*.

(13) Fossdal, A.; Menon, M.; Wærnhus, I.; Wiik, K.; Einarsrud, M.; Grande, T. *J. Am. Ceram. Soc.* **2004**, *87*, 1952.

(14) Gale, J. D.; Rohl, A. L. *Mol. Simul.* **2003**, *29*, 291.

(15) Islam, M. S. *J. Mater. Chem.* **2000**, *10*, 1027.

(16) Catlow, C. R. A. *Computer Modelling in Inorganic Crystallography*; Academic Press: San Diego, CA, 1997.

(17) Dick, B. G.; Overhauser, A. W. *Phys. Rev.* **1958**, *112*, 90.

(18) Mott, N. F.; Littleton, M. J. *Trans. Faraday Soc.* **1938**, *34*, 485.

(19) Cherry, M.; Islam, M. S.; Catlow, C. R. A. *J. Solid State Chem.* **1995**, *118*, 125.

(20) Falcón, H.; Goeta, A. E.; Punte, G.; Carbonio, R. E. *J. Solid State Chem.* **1997**, *133*, 379.

(21) Lewis, G. V.; Catlow, C. R. A. *J. Phys. C: Solid State Phys.* **1985**, *18*, 1149.

(22) Khan, M. S.; Islam, M. S.; Bates, D. R. *J. Phys. Chem. B* **1998**, *102*, 3099.

(23) Driscoll, D. J.; Islam, M. S.; Slater, P. R. *Solid State Ionics* **2005**, *176*, 539. French, S. A.; Catlow, C. R. A.; Oldman, R. J.; Rogers, S. C.; Axon, S. A. *Chem. Commun.* **2002**, *22*, 2706. Islam, M. S.; Driscoll, D. J.; Fisher, C. A. J.; Slater, P. R. *Chem. Mater.* **2005**, *17*, 5085. Levy, M. R.; Steele, B. C. H.; Grimes, R. W. *Solid State Ionics* **2004**, *175*, 349.

(24) Kröger, F. A. *The Chemistry of Imperfect Crystals*; Interscience (Wiley): Amsterdam, 1974.

(25) Wærnhus, I.; Grande, T.; Wiik, K. *Solid State Ionics* **2005**, *176*, 2609.

(26) Fisher, C. A. J.; Islam, M. S. *J. Mater. Chem.* **2005**, *15*, 3200. Read, M. S. D.; Islam, M. S.; Watson, G. W.; King, F.; Hancock, F. E. *J. Mater. Chem.* **2000**, *10*, 2298.

(27) Chainani, A.; Mathew, M.; Sarma, D. D. *Phys. Rev. B* **1993**, *48*, 14818. Abbate, M.; Degroot, F. M. F.; Fuggle, J. C.; Fujimori, A.; Strebel, O.; Lopez, F.; Domke, M.; Kaindl, G.; Sawatzky, G. A.; Takano, M.; Takeda, Y.; Eisaki, H.; Uchida, S. *Phys. Rev. B* **1992**, *46*, 4511. Chang, C. L.; Chern, G.; Tai, M. F.; Su, Y. W.; Dong, C. L.; Liu, S. Y.; Hwang, C. S.; Tseng, P. K. *Jpn. J. Appl. Phys., Part 1* **1999**, *38*, 108. Jung, W. H.; Iguchi, E. *J. Phys.: Condens. Matter* **1995**, *7*, 1215.

(28) Tealdi, C.; Malavasi, L.; Fisher, C. A. J.; Islam, M. S. *J. Phys. Chem. B* **2006**, *110*, 5395.

(29) Huang, K.; Lee, H. Y.; Goodenough, J. B. *J. Electrochem. Soc.* **1998**, *145*, 3220. Ishihara, T.; Matsuda, H.; Takita, Y. *J. Am. Chem. Soc.* **1994**, *116*, 3801.

(30) Mizusaki, J.; Yasuda, I.; Shimoyama, J.; Yamauchi, S.; Fueki, K. *J. Electrochem. Soc.* **1993**, *140*, 467.

(31) Kilner, J. A. *Solid State Ionics* **2000**, *129*, 13.

(32) Norby, T. *J. Mater. Chem.* **2001**, *11*, 11.

(33) Nowick, A. S.; Fu, S. Q.; Lee, W. K.; Lim, B. S.; Scherban, T. *Mater. Sci. Eng., B* **1994**, *23*, 19.

(34) Islam, M. S.; Davies, R. A. *J. Mater. Chem.* **2004**, *14*, 86.

(35) Patrakeev, M. V.; Bahteeva, J. A.; Mitberg, E. B.; Leonidova, I. A.; Kozhevnikov, V. L.; Poeppelmeier, K. R. *J. Solid State Chem.* **2003**, *172*, 219.

(36) Haavik, C.; Ottesen, E. M.; Nomura, K.; Kilner, J. A.; Norby, T. *Solid State Ionics* **2004**, *174*, 233.

(37) Skowron, A.; Huang, P. N.; Petric, A. *J. Solid State Chem.* **1999**, *143*, 202.

(38) Huang, K. Q.; Tichy, R. S.; Goodenough, J. B. *J. Am. Ceram. Soc.* **1998**, *81*, 2565.

(39) Mather, G. C.; Islam, M. S. *Chem. Mater.* **2005**, *17*, 1736.

(40) Günter, M. M.; Boysen, H.; Corte, C.; Lerch, M.; Suard, E. *Z. Kristallogr.* **2005**, *220*, 218. Lerch, M.; Boysen, H.; Hansen, T. *J. Phys. Chem. Solids* **2001**, *62*, 445. Yashima, M.; Nomura, K.; Kageyama, H.; Miyazaki, Y.; Chitose, N.; Adachi, K. *Chem. Phys. Lett.* **2003**, *380*, 391.

(41) Ishigaki, T.; Yamauchi, S.; Mizusaki, J.; Fueki, K.; Naito, H.; Adachi, T. *J. Solid State Chem.* **1984**, *55*, 50.

(42) Berenov, A.; Wei, J.; Wood, H.; Rudkin, R.; Atkinson, A. *J. Solid State Electrochem.* **2007**, *11*, 482. Waller, D.; Lane, J. A.; Kilner, J. A.; Steele, B. C. H. *Solid State Ionics* **1996**, *86−88*, 767.

(43) Tietz, F.; Haanappel, V. A. C.; Mai, A.; Mertens, J.; Stover, D. *J. Power Sources* **2006**, *156*, 20.

(44) Berenov, A. V.; MacManus-Driscoll, J. L.; Kilner, J. A. *Solid State Ionics* **1999**, *122*, 41.

(45) Stevenson, J. W.; Hallman, P. F.; Armstrong, T. R.; Chick, L. A. *J. Am. Ceram. Soc.* **1995**, *78*, 507. Schulz, O.; Martin, M.; Argirusis, C.; Borchardt, G. *Phys. Chem. Chem. Phys.* **2003**, *5*, 2308.

(46) Wolfenstine, J. *Solid State Ionics* **1999**, *126*, 293.

(47) Martin, M. *Solid State Ionics* **2000**, *136*, 331.

(48) De Souza, R. A.; Maier, J. *Phys. Chem. Chem. Phys.* **2003**, *5*.

(49) De Souza, R.; Islam, M. S.; Ivers-Tiffee, E. *J. Mater. Chem.* **1999**, *9*, 1621.

(50) Smith, J. B.; Norby, T. *Solid State Ionics* **2006**, *177*, 639.

(51) Kilo, M.; Taylor, M. A.; Argirusis, C.; Borchardt, G.; Jackson, R. A.; Schulz, O.; Martin, M.; Weller, M. *Solid State Ionics* **2004**, *175*, 823.